Monthly Notices
of the
ROYAL ASTRONOMICAL SOCIETY

MNRAS **478,** 2557–2568 (2018)
Advance Access publication 2018 May 3

doi:10.1093/mnras/sty1134

Eleven years of monitoring the Seyfert 1 Mrk 335 with *Swift*: Characterizing the X-ray and UV/optical variability

L. C. Gallo,[1]★ D. M. Blue,[1,2] D. Grupe,[3] S. Komossa[4] and D. R. Wilkins[5]

[1]*Department of Astronomy and Physics, Saint Mary's University, 923 Robie Street, Halifax, NS, B3H 3C3, Canada*
[2]*Department of Mathematics, Mount Saint Vincent University, 166 Bedford Hwy, Halifax, NS B3M 2J6, Canada*
[3]*Space Science Center, Morehead State University, 235 Martindale Drive, Morehead, KY 40351, USA*
[4]*Max-Planck-Institut für Radioastronomie, Auf dem Hügel 69, D-53121 Bonn, Germany*
[5]*Kavli Institute for Particle Astrophysics and Cosmology, Stanford University, Stanford, CA, 94305, USA*

Accepted 2018 April 30. Received 2018 April 30; in original form 2018 March 15

ABSTRACT

The narrow-line Seyfert 1 galaxy (NLS1) Mrk 335 has been continuously monitored with *Swift* since May 2007 when it fell into a long-lasting, X-ray low-flux interval. Results from nearly 11 years of monitoring are presented here. Structure functions are used to measure the UV-optical and the X-ray power spectra. The X-ray structure function measured between 10 and 100 d is consistent with the flat, low-frequency part of the power spectrum measured previously in Mrk 335. The UV-optical structure functions of Mrk 335 are comparable with those of other Seyfert 1 galaxies and of Mrk 335 itself when it was in a normal bright state. There is no indication that the current X-ray low-flux state is attributed to changes in the accretion disc structure of Mrk 335. The characteristic time-scales measured in the structure functions can be attributed to the thermal (for the UV) and the dynamic (for the optical) time-scales in a standard accretion disc. The high-quality UVW2 (∼1800 Å in the source frame) structure function appears to have two breaks and two different slopes between 10 and 160 d. Correlations between the X-ray and other bands are not highly significant when considering the entire 11-yrlight curves, but more significant behaviour is present when considering segments of the light curves. A correlation between the X-ray and the UVW2 in 2014 (Year-8) may be predominately caused by a giant X-ray flare that was interpreted as a jet-like emission. In 2008 (Year-2), possible lags between the UVW2 emission and other UV-optical waveband may be consistent with reprocessing of X-ray or UV emission in the accretion disc.

Key words: galaxies: active – galaxies: individual: Mrk 335 – galaxies: nuclei – X-rays: galaxies.

1 INTRODUCTION

The narrow-line Seyfert 1 galaxy (NLS1) Mrk 335 ($z = 0.025$) has been the subject of intense scrutiny (e.g. Grupe et al. 2008; Longinotti et al. 2008, 2013; Gallo et al. 2013, 2015; Wilkins et al. 2015) since it was discovered in a historically low X-ray flux state in 2007 (Grupe, Komossa & Gallo 2007). After decades of being one of the brightest active galactic nuclei (AGN) in the X-ray sky, Mrk 335 initially faded to about one-thirtieth of its typical brightness. Since that substantial drop, Mrk 335 has never fully recovered to its previous bright state. *Swift* monitoring with the *X-ray Telescope* (*XRT*) and the *UV-Optical Telescope* (*UVOT*) over the past 11 years finds the source to be highly variable in the X-rays, showing persistent variability and occasional intense flaring by factors of 10. However, on an average, the source remains about one-tenth of its previous brightness and this low state appears to be the new normal for Mrk 335 (Grupe et al. 2012). It is not clear if the change in behaviour arises from some physical change in the accretion process (e.g. akin to state changes in stellar mass black holes) or simply those produced in a stationary process.

In the optical-to-UV bands the source is one of the most persistently variable radio-quiet AGN changing in brightness by factors of ∼2 (e.g. Peterson et al. 1998; Grupe et al. 2012; Komossa et al. 2014). However, during this X-ray dim phase, the average optical/UV brightness has not changed significantly compared to historical values. Compared to its UV luminosity, Mrk 335 is now in an X-ray weak state (e.g. Gallo 2006). The substantial dimming of the AGN is only evident in the X-rays. The origin of the X-ray dimming remains uncertain and explanations have included the collapse of the corona perhaps forming a collimated structure (e.g. Gallo et al. 2013, 2015; Wilkins & Gallo 2015; Wilkins et al. 2015)

★ E-mail: lgallo@ap.smu.ca

or absorption and partial obscuration of the disc and corona (e.g. Grupe et al. 2008; Longinotti et al. 2013). While partial covering has difficulty describing the broad-band low- and high-flux intervals in a self-consistent manner (Gallo et al. 2015), and the reverberation lags seen in some flux states (Kara et al. 2013), there is an indication in a new *XMM–Newton* observation that obscuration may play a role in the low-flux state (Longinotti et al. in prep; Gallo et al. in prep).

The long-term, multi-wavelength monitoring campaign of Mrk 335 with *Swift* has not been examined to the same degree as the X-ray data (see Grupe et al. 2012; Komossa et al. 2017). The UV emission is the dominant component in the spectral energy distribution (SED) of AGN, attributed to the accretion disc that feeds the supermassive black hole. Changes in the accretion disc structure or flow could explain the weak corona emission we now see in Mrk 335.

The first five years of the monitoring campaign are presented by Grupe et al. (2012). In this work, we look at the entire 11-yr monitoring campaign of Mrk 335 that was initiated in 2007 (Grupe et al. 2007) with the goal of characterizing the optical/UV emission in the NLS1. The *Swift* light curves have significant data, but are sampled infrequently because of observing constraints throughout the year. Therefore, we use appropriate techniques such as structure function analysis to examine power spectra and characteristic time-scales (e.g. Hughes, Aller & Aller 1992; Collier & Peterson 2001), and discrete correlation functions (Edelson et al. 1988) to investigate correlations and lags.

In the next section the observations and the data processing are described. The light curves and amplitude of the variations are presented in Section 3. The structure function of each light curve is derived in Section 4 and the discrete correlation functions are determined in Section 5. Discussion and conclusions follow in Section 6 and Section 7, respectively. Analysis of the SED and spectral variability are saved for future work.

2 OBSERVATIONS AND DATA REDUCTION

Mrk 335 has been the target of a continuous survey since May 2007 when it was discovered in an extremely low X-ray flux state (Grupe et al. 2007). Here the extremely long (nearly 11 years) *Swift* monitoring of Mrk 335 between 2007 May 17 and 2017 December 31 is reported and the associated optical, UV, and X-ray (0.3−10 keV) light curves are presented. The observations were only interrupted during the three month period between February and May, when Mrk 335 was in sun constraint with *Swift*. The observation log listing all observation between 2012 January and 2018 January is provided in Table 1. The log showing data between 2007 and 2011 was shown previously in Grupe et al. (2012).

In order to avoid filter rotations on *Swift UVOT* (Roming et al. 2005), most observations were performed with a 4 or 8 d cadence when the UVW2 (1928 Å) filter was 'Filter of the Day', which is a method to reduce filter wheel rotation in order to extend the *UVOT* lifetime. The X-ray and the *UVOT* UVW2 light curves have good sampling over the ∼11 years. Observations in the other five *UVOT* filters [V (5468 Å), B (4392 Å), U (3465 Å), UVW1 (2600 Å), and UVM2 (2246 Å)] are more sparse. Only at the beginning of the monitoring campaign in 2007 and 2008 was there good coverage in all six *UVOT* filters.

All observations with the *Swift XRT* (Burrows et al., 2005) were performed in a photon-counting mode (pc, Hill et al., 2004), except for a short period in 2014, between September 17 and October 06, when it was observed in a Windowed Timing (WT) mode during an X-ray flare event. *XRT* data were reduced with the task XRTPIPELINE version 0.13.4., which is included in the HEASOFT package 16.1. For each observation we extracted source and background spectra and event files using XSELECT. Source counts were extracted from a circular region with a radius of 94 arcsec and the background counts were from a source-free, circular region with a radius 295 arcsec. We created auxiliary response files (ARF) for each of these spectra using the FTOOL XRTMKARF. The most recent response files swxpc0to12s6_20130101v014.rmf for the pc data and swxwt0to2s6_20131212v015.rmf for the WT data were adopted.

The *UVOT* data of each observation were co-added in each filter with the *UVOT* task UVOTIMSUM. Source counts were selected from a circular region with a radius of 5 arcsec and the background counts were extracted from a circular region with a radius of 20 arcsec close to the source. *UVOT* magnitudes and flux densities were measured with the task UVOTSOURCE based on the most recent *UVOT* calibration as described in Poole et al. (2008) and Breeveld et al. (2010). The *UVOT* data were corrected for Galactic reddening ($E = 0.035$; Schlegel, Finkbeiner & Davis 1998), using equation (2) in Roming et al. (2009) and reddening curves from Cardelli, Clayton & Mathis (1989). No correction has been made for host-galaxy contamination, consequently, the variability in the optical wavebands (e.g. B, V) will be diluted.

The *XRT* and *UVOT* measurements, including hardness ratios, for each observation between January 2012 and 2018 are shown in Table 2. The measurements prior to 2012 were listed in Grupe et al. (2012). All uncertainty values in the tables and figures correspond to 1σ error bars unless specified otherwise. The time-scales are reported in the observed frame. Given the low redshift of Mrk 335, the difference between frames is negligible compared to the timing resolution used in this work.

3 LIGHT CURVES AND FRACTIONAL VARIABILITY

The *Swift* light curves between 2007 May and 2017 December are shown for each waveband in Fig. 1. In each year (e.g. observing campaign), Mrk 335 is visible to *Swift* for approximately 250 d before it is in sun constraint. The cadence of the observations depends on the filter used. The X-rays (0.3−10 keV) and UVW2 are the preferred combination and the typical sampling rate is between 4 and 8 d during an observing year. However, increased monitoring is requested at times and some parts of the light curve may even be sampled daily. The other optical/UV filters are used less frequently. Data obtained since 2012 January are presented in Table 1 and 2 (full tables are available online). Data obtained prior to 2012 are available from Grupe et al. (2008, 2012).

The light curves exhibit significant variability in each waveband with the largest fluctuations apparent in the X-ray. The minimum-to-maximum X-ray count rate varies by a factor of ∼50 over the 11 years from ∼0.03 to ∼1.54 count s^{-1} .

To estimate the amplitude of the variations in each waveband, the fractional variability (F_{var}) and the uncertainties are calculated following Edelson et al. (2002). The F_{var} for the entire 11-yrdata set shows the amplitude of the variations increase with energy (Fig. 2). The X-ray band is significantly more variable than the UV and the optical bands. The F_{var} decreases from ∼20 per cent in the UVW2 filter to ∼7 per cent in the *V* band. This diminished variability at longer wavelengths likely results from a combination of increased host-galaxy contamination and decreased intrinsic variability. Since the amplitude of the variations in the UV and optical is small

Table 1. *Swift XRT* and *UVOT* observations of Mrk 335 since 2012 January. All exposures are given in seconds. Observations prior to 2012 are listed in Grupe et al. (2008) and (2012). The full list of observations is shown online.

ObsID	Segment	$T_{\rm start}$ (UT)	$T_{\rm end}$ (UT)	MJD	$T_{\rm exp,\,XRT}$	$T_{\rm exp,\,V}$	$T_{\rm exp,\,B}$	$T_{\rm exp,\,U}$	$T_{\rm exp,\,W1}$	$T_{\rm exp,\,M2}$	$T_{\rm exp,\,W2}$
35755	092	55946.819	2012-01-20 19:33	2012-01-20 19:48	919	—	—	—	—	—	924
	093	55947.828	2012-01-21 19:51	2012-01-21 19:51	25	—	—	—	—	—	37
	094	55948.625	2012-01-22 14:51	2012-01-22 15:08	976	—	—	—	—	—	985
	095	55949.896	2012-01-23 21:22	2012-01-23 21:39	976	—	—	—	—	—	973
	096	55950.965	2012-01-24 23:01	2012-01-24 23:17	954	—	—	—	—	—	948

Table 2. *Swift XRT* and *UVOT* measurements of Mrk 335 since 2012 January. The *XRT* values are in units of counts s^{-1}. The hardness ratio is defined as $HR = \frac{hard-soft}{hard+soft}$ where soft and hard are the counts in the 0.3–1.0 keV and 1.0–10.0 keV bands, respectively. The reddening-corrected *UVOT* magnitudes are in the Vega system. Measurements prior to 2012 are listed in Grupe et al. (2008) and (2012). The full list of observations is shown online.

MJD	XRT CR	XRT HR	V	B	U	UVW1	UVM2	UVW2
55946.819	0.576 ± 0.027	-0.13 ± 0.05	—	—	—	—	—	12.72 ± 0.03
55947.828	—	—	—	—	—	—	—	12.71 ± 0.03
55948.625	0.367 ± 0.021	-0.05 ± 0.05	—	—	—	—	—	12.75 ± 0.03
55949.896	0.912 ± 0.044	-0.03 ± 0.06	—	—	—	—	—	12.78 ± 0.03
55950.965	0.886 ± 0.038	-0.12 ± 0.05	—	—	—	—	—	12.82 ± 0.03
55951.098	0.678 ± 0.032	-0.05 ± 0.05	—	—	—	—	—	12.82 ± 0.03

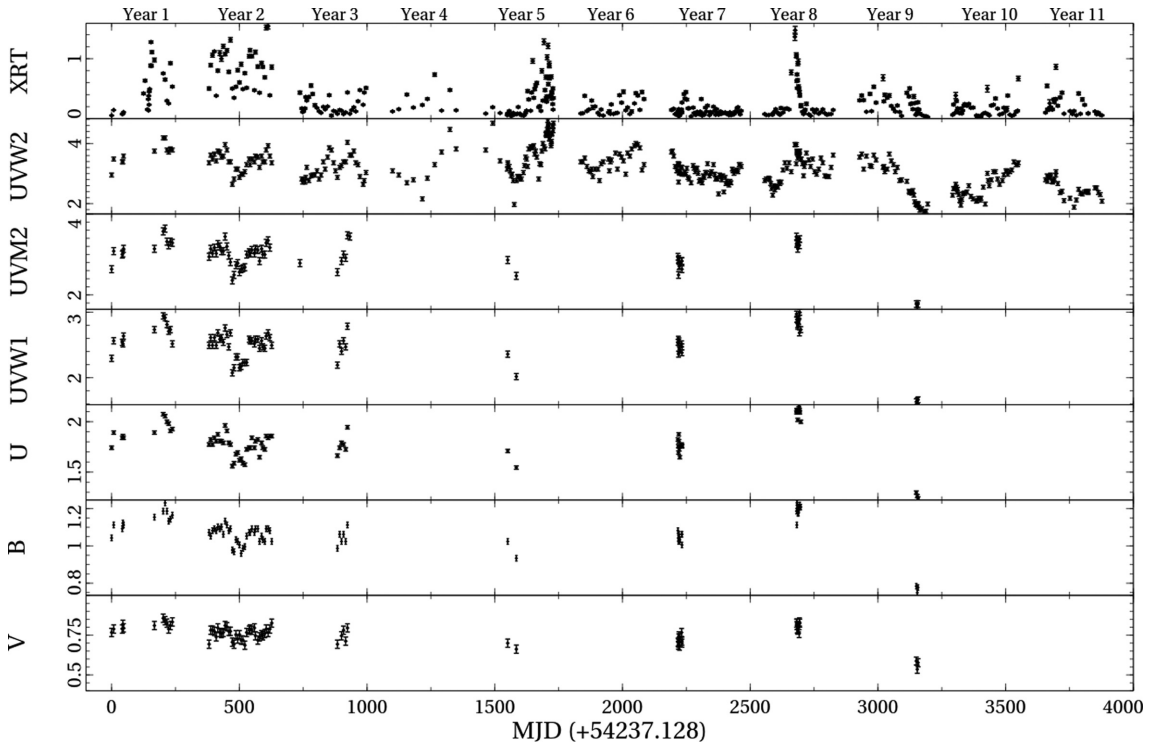

Figure 1. The *Swift XRT* (0.3−10 keV) and *UVOT* light curves for Mrk 335 from 2007 May 17 to 2017 December 31. Data from specific epochs are referred to by 'Year' as defined in the top row and distinguished by the ∼3 month gap where Mrk 335 is in sun constraint with *Swift*. The data presented by Grupe et al. (2012) are prior to MJD∼54237 + 1750 (i.e. approximately Year 1 to Year 5). The *XRT* light curve is in counts s^{-1}. *UVOT* flux densities are expressed in units of 10^{-14} erg s^{-1} cm^{-2} $Å^{-1}$. Error bars in the brightness are present on all data.

compared to X-rays (Fig. 2), the signals (e.g. correlations and delays) searched for in the analysis are expected to be weak.

The fractional variability is calculated for each waveband in each observing year, for which at least six observations were obtained. All wavebands exhibit a common trend in which the $F_{\rm var}$ diminishes with increasing flux (Fig. 3), which is indicative of a stationary process. However, there is a significant scatter in how $F_{\rm var}$ changes with flux and time. This does not necessarily indicate changes in the underlying physical processes generating the energy. The measured fractional variability does depend on the sampling in a given filter, which does vary from year-to-year. This likely contributes to the significant scatter present in the $F_{\rm var}$-flux trend in all filters. A

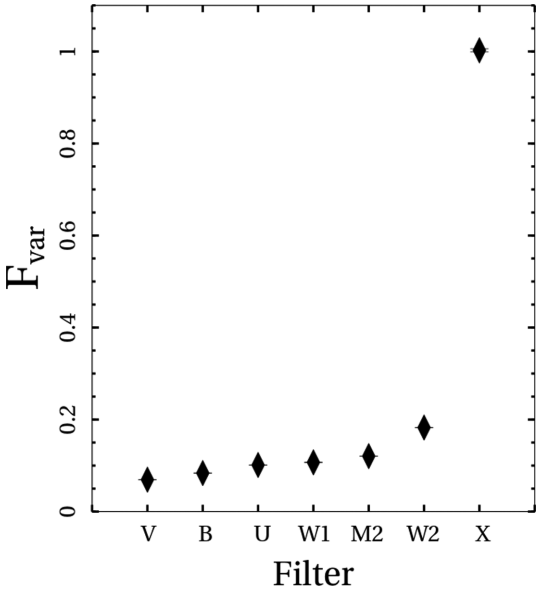

Figure 2. The fractional variability of Mrk 335 measured in each waveband (shown in increasing energy). Uncertainties are plotted, but appear smaller than the data points.

stationary process dominated by red noise will exhibit differences in the mean and the variance with time (e.g. Vaughan et al. 2003).

4 STRUCTURE FUNCTION ANALYSIS

4.1 The structure function

The power spectral density (PSD; power spectrum) shows the distribution of variability power in a light curve as a function of frequency. For AGN, the power spectrum follows a power-law shape [$P(f) \propto f^{-\alpha}$, where P is the power and f is the temporal frequency], with index $\alpha \sim 2$ (i.e. red noise) (e.g. McHardy et al. 2004; Arévalo, McHardy & Summons 2008; Breedt et al. 2010). Towards lower frequencies (longer time-scales), the spectrum will flatten ($\alpha \sim 1$). The break or characteristic frequency (f_b) is attributed to some underlying physical process and scales with the black hole mass and the accretion rate (e.g. McHardy et al. 2006). There is also an indication that it may be linked to the line-of-sight absorption in the source (González-Martín 2018). Work on stellar mass black hole binaries shows that the variability in the shape of the power spectrum can be used to reveal underlying changes in the behaviour of the accretion system that are not easily disclosed with a fractional variability analysis.

The Mrk 335 data set is rich, but it is inhomogeneous and the sampling is uneven over the course of a year. Therefore, using Fourier-transform techniques, such as the PSD, is possible, but can be problematic. For this work, the distribution of power in the light curves is examined using a structure function analysis (SF; e.g. Simonetti, Cordes & Heeschen 1985; Hughes et al. 1992; Di Clemente et al. 1996).

The method of SF analysis to study the variability of ensembles and individual AGN is widely used (e.g. Simonetti et al. 1985; Hughes et al. 1992; Di Clemente et al. 1996; Vanden Berk et al. 2004; Bauer et al. 2009; Vagnetti et al. 2016; Middei et al. 2017). Collier & Peterson (2001, hereafter CP01) apply the method to study the UV/optical variability in a sample of Seyfert galaxies including Mrk 335.

The SF can be used in the same manner as a PSD to evaluate the distribution of power in a time series. The primary difference is that the structure function operates in the time domain and can be used effectively to examine irregularly sampled light curves like those in this work. Specifically, the SF is a function of time differences ($\tau = t_j - t_i$) between pairs of points, i and j (where $j > i$), in a series with $N(\tau)$ pairs. The definition used by CP01 is adopted here to ease comparison to that work. That is

$$SF(\tau) = \frac{1}{N(\tau)} \sum_{i<j} [f(t_i) - f(t_i + \tau)]^2 \quad (1)$$

Between some minimum and maximum time-scale where the variations are correlated, the SF will take on a power-law shape. Like the PSD, the slope of the spectrum encodes information of the accretion process and for a stationary light curve the PSD slope is related to the slope of the SF (β) by $\alpha = \beta + 1$ (Hufnagel & Bregmann 1992; Kawaguchi et al. 1998). However, Paltani (1999) note this is only valid for an infinite time series.

At long time-scales the SF will begin to flatten at approximately two times the time series variance ($2\sigma^2$) (Hughes et al. 1992). The turnover occurs at some characteristic time-scale (τ_{char}) that is related to the break frequency in the PSD. The power law also flattens at short time-scales where the signal is approximately two times the noise variance ($2\sigma_n^2$) (Hughes et al. 1992). However, the flattening could also be an artefact of a finite, non-stationary light curve.

CP01 test if the observed flattening in the SF could be attributed to the physical processes and if the power-law slope (β) could be related to the PSD slope (α). CP01 find that a power-law slope is expected at times $\lesssim 0.3T$, where T is the duration of the light curve. Any flattening occurring at time-scales less than $0.3T$ may represent flattening from intrinsic AGN processes. Likewise, the power-law slope can be used to predict the PSD spectral index as noted above, but sampling and binning of the structure function may invalidate the relation. CP01 estimate the systematic uncertainty to be at 10 per cent level so the simple relation between α and β can be used as an approximation.

The method employed in this work is same as that of CP01. The binned SF is calculated using equation (1). Binning is achieved such that the midpoint of bin i is at $\tau_i = (i - \frac{1}{2})\delta$, where δ is the resolution of the structure function taken to be the median temporal sampling of the light curve with duration T. The SF is only calculated for bins with more than six light curve pairs. The number of bins for each SF is $\frac{T}{\delta+1}$. Two times the mean noise variance is subtracted from each SF bin to remove the effects of the measurement uncertainties. This will also result in the flat plateau at the short time-scales to be minimized in the SF. Finally, the SF is then normalized to the light curve variance to ease comparison to CP01. Again following CP01, the statistical uncertainties in the SF are defined as $\frac{\sigma_i}{\sqrt{N_i/2}}$, where N_i is the number of pairs in bin i and σ_i is the root mean square deviations about the mean SF value in that bin.

4.2 Optical and UV structure functions

The structure functions for the approximately 11-yr light curves of Mrk 335 in the *UVOT* bands are shown in Fig. 4. All the SFs, except for the *V*-band, exhibit the power-law slope with the flattening at long time-scales before oscillations arise at time-scales when the SFs are poorly defined. The flattening at short time-scales is less obvious as the measurement uncertainties were subtracted

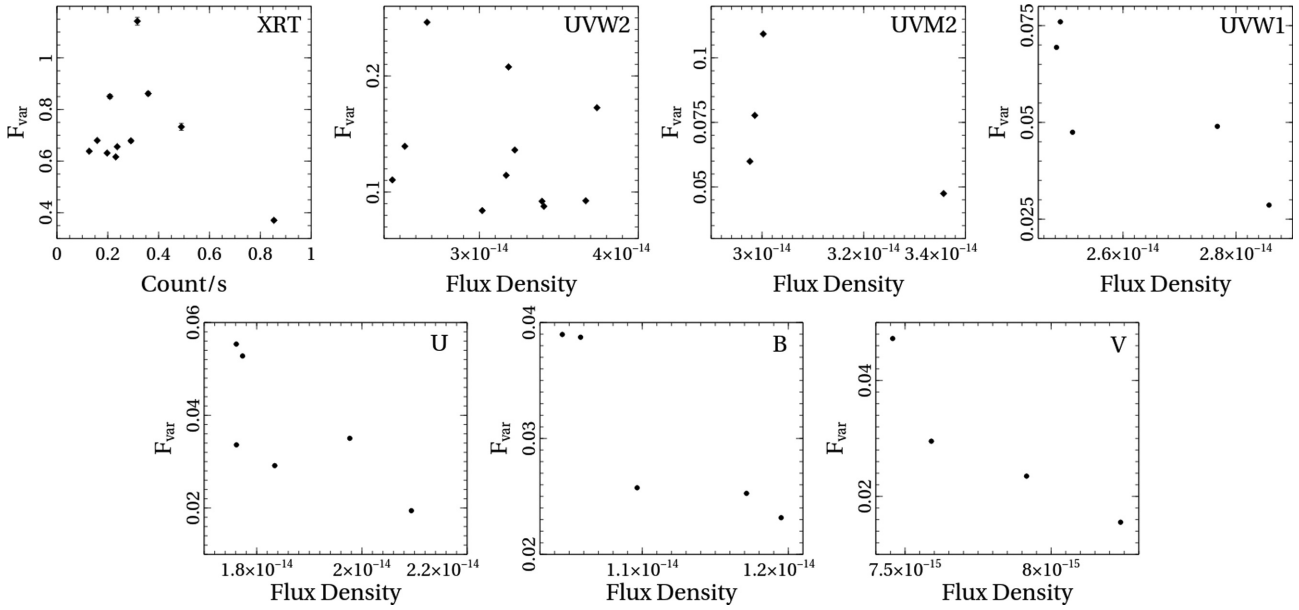

Figure 3. The fractional variability of Mrk 335 measured in each waveband plotted against the mean flux during that observing year. Each data point corresponds to a single campaign (year) in which at least six observations were completed. Uncertainties are plotted, but appear smaller than the data points. *UVOT* flux densities are expressed in units of erg s^{-1} cm^{-2} Å^{-1}.

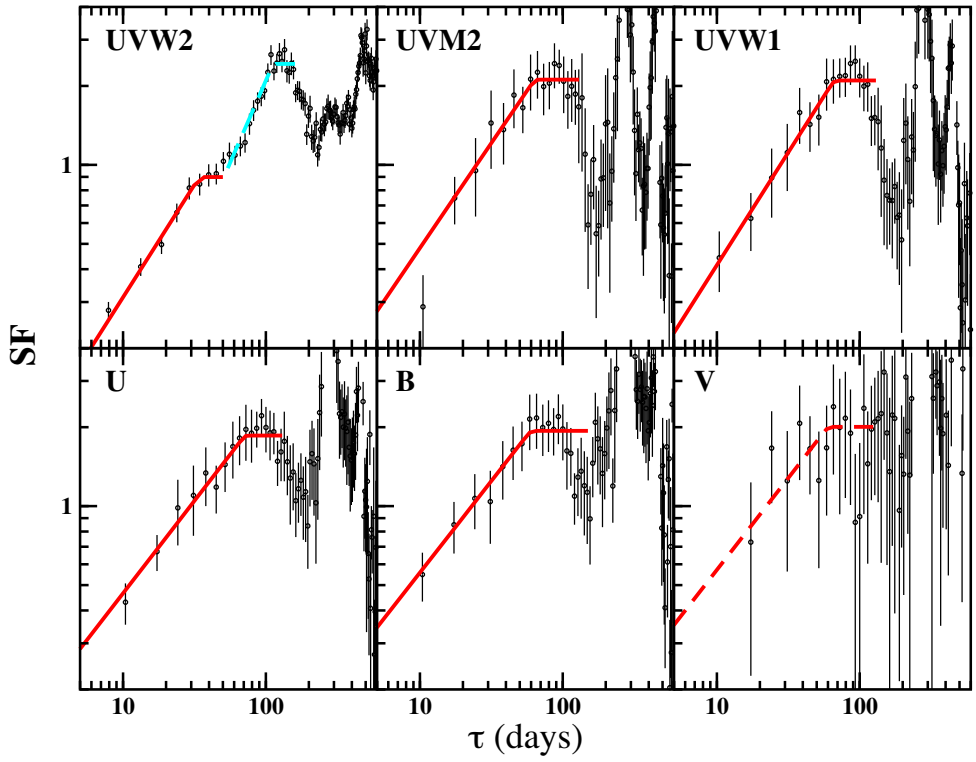

Figure 4. Broken power laws fitted to the structure functions of the *Swift UVOT* observations of Mrk 335. The typical SF shows a power-law slope with increasing τ before flattening. The flattening continues briefly before the onset of the oscillations in the noise-dominated regime of the SF. For clarity, the data are only shown up to $\tau = 600$ d. Two fits of the structure function are made for the UVW2 data. (a) Corresponds to fitting the SF between 10 and 50 d (red solid model in the top-left panel) and (b) corresponds to fitting the data between 50 and 160 d (dashed cyan model in the top-left panel) to demonstrate the possibility of two distinct slopes and characteristic time-scales in the UVW2 SF. A fit to the *V*-band data could not be well constrained. The model shown (dashed red curve) corresponds to the *B*-band SF fit.

when building the SFs. However, there may be some indication of flattening in some SF at $\tau < 10$ d.

The power-law shape is well defined in all SFs except for the *V*-band. Between τ_{min} (taken to be 10 d for all SFs) and τ_{max} ($\gtrsim$100d), each structure function is fitted with a broken power law where the break is the transition between the sloped and the flat part of the function. The break time-scale is defined as the characteristic time-scale (τ_{char}). The slope above τ_{char} is fixed at 0 to ease the fitting process. Determining the break time-scale is rather subjective because the flat part of the SF is of short duration before the function becomes noise dominated (i.e. the oscillations set in). Therefore, the values of τ_{char} should be considered with caution. The power law and the characteristic time-scale are always measured over a range that is $<0.3T$, thus the results should be robust to biases discussed in Section 4. The characteristics of each SF and the fit results are shown in Table 3. In the final column of Table 3, the corresponding PSD slope is listed assuming $\alpha = \beta + 1$ as discussed above.

The *V*-band light curve is crudely sampled and exhibits the weakest variability (i.e. lowest $F_{\rm var}$), thus the poorly defined SF is not surprising. The broken power law could not be fitted to the data. In Fig. 4, the *V*-band SF is shown with the *B*-band model overplotted. Since the V and B are adjacent bandpasses, the SFs are expected to be similar as appears to be the case (Fig. 4).

The values of the SF slope are $\sim$0.71 for the optical bands (U, B, and V) and $\sim$0.80 for the UV bands [UVW2 between ($\tau = 10-50$ d), UVM2, UVW1] though all measurements agree within uncertainties. This is suggestive of a similar physical process driving the variations in the optical and the UV bands. The corresponding PSD slopes are $\sim$1.7$-$1.8, which are typical of most Seyfert 1 galaxies, though there are exceptions (e.g. Mushotzky et al. 2011). The characteristic time-scale is about 60 d though there is a large range on the uncertainty on each individual measurement.

Interestingly, the high-quality data in the UVW2 light curve reveals complexity in its SF (Fig. 4, top left). There is evidence of multiple breaks and different slopes in the power spectrum. Fitting a broken power law between 10 and 50 d reveals a slope of $\beta \approx 0.86$ and a break at about 35 d. Between 50$-$160 d, the slope is steeper ($\beta \approx 1.25$) and a second break is evident at $\tau_{char} \approx 112$ d. Multiple breaks were also seen in the optical SF of NGC 5506 (CP01).

4.3 X-ray structure function

The X-ray structure function is different than the UV/optical ones (Fig. 5). The function is significantly flatter ($\beta = 0.14 \pm 0.05$) and there is no measurable evidence of a break in the power law before oscillations set in at $\sim$120 d. It may even be possible that the oscillations start sooner seeing the two SF bins below 100 d that are outliers to the fit.

The SF is examined between 10 and 100 d and these are sufficiently low frequencies that the break likely occurs at much shorter time-scales (higher frequencies). Arévalo et al. (2008) measure a low-frequency break in Mrk 335 at $\sim 1.6 \times 10^{-4}$Hz ($\sim$0.07 d) so it could be that we are not examining the steep part of the power spectrum in the X-rays. The low-frequency slope in the PSD measured by Arévalo et al. (2008) is $\sim$1.1, which agrees with our SF measurement of β that would correspond to $\alpha \approx 1.14$. While the *Swift* X-ray sampling is not probing the linear part of the SF, the low-frequency behaviour is consistent with a PSD slope of $\sim$1. Analysis of the X-ray power spectrum would improve by examining the long *XMM–Newton* observations with more frequent sampling on the order of hours and days.

5 DISCRETE CORRELATION FUNCTION

The correlations between light curves is examined over the entire $\sim$11-yr period as well as within each of the yearly observing campaigns. Year 2 (Fig. 1) is fruitful to examine correlations among all the *UVOT* filters since the light curves were well sampled in all wavebands in that epoch.

Given the irregular sampling in the time series, the Discrete Correlation Function (DCF; Edelson & Krolik 1988) is employed to investigate correlations between light curves.[1] Monte Carlo confidence intervals are determined for each DCF. A PSD slope of $\alpha = 1.2$ (see Section 4) is adopted to generate 10^5 random X-ray light curves (Timmer & König 1995) with similar binning and cadence to the true X-ray data. Gaps are inserted in the light curves to simulate the periods of sun constraint in the real data. Artificial X-ray light curves are compared with the true optical-UV light curves and the DCF coefficients are determined at each lag interval. A cumulative distribution of the DCF coefficients is constructed to determine the 95 and the 99.9 per cent coefficients that are shown in the plots. The process is similar for generating UVW2 light curves that are compared to the other *UVOT* light curves in Year 2.

5.1 Correlations with X-rays over the 11 years

The DCFs between the X-ray light curve and each UV-optical waveband for the entire 11-yr monitoring campaign are shown in Fig. 6. The peak correlation is significant at $\sim$95 per cent confidence for all wavebands, but never reaches the 99.9 per cent confidence contour.

The X-ray and the UVW2 light curves exhibit a DCF peak at approximately zero lag. However, for all other wavebands, the DCFs exhibit an asymmetry towards a positive lag. The peaks are at 5 ± 5 days, that corresponds to one resolution element and are formally consistent with zero.

The similarity suggests that a short lag does exist, such that the X-rays lead the UV-optical bands, but light curves with higher time resolution are required, as implied by Arévalo et al. (2008). This may be an indication of the reprocessing of X-rays in the accretion disc (e.g. Cameron et al. 2012; Shappee et al. 2014; McHardy et al. 2014).

5.2 A comparison between the X-ray and the UVW2 light curves in each year

The UVW2 light curve is the best sampled of all the optical-UV wavebands. Given the good simultaneous sampling between the X-rays and the UVW2 light curves, the DCF for this pair can be calculated for each individual year. The errors on the DCF are rather large for Years 1 and 4, when there are limited data, so little can be said of those epochs. For the remaining epochs, the correlations during each individual year do not exceed the 95 per cent confidence level except for Year 8 (Fig. 7).

Like many of the DCFs in the 11-yr average (Fig. 6), the DCF in Year 8 exhibits a peak at a positive lag between 0 and 10 d, but only in this case is the significance of the correlation at the $\sim$99.9 per cent confidence level (Fig. 7). Similar to the 11-yr average, the lag is consistent with the X-rays leading the UV band.

Notably, Year 8 (2014) corresponds to when Mrk 335 displayed a giant X-ray flare accompanied by more modest brightening in the

[1] The code developed by Robertson et al. (2015) is used to calculate the DCF and errors following Edelson & Krolik (1988).

Table 3. The *Swift UVOT* and *XRT* structure function parameters measured for Mrk 335. The waveband is given in column (1) followed by total observation length T and structure function resolution δ in columns (2) and (3), respectively. Column (4) and (5) are the minimum (τ_{min}) and maximum (τ_{max}) time lag over which the broken power law model is fit. The measured parameters of the structure function are the power-law slope (β ; column 6) and the break in the power law (i.e. characteristic time-scale) (τ_{char}; column 7), where the break occurs in the SF power law. The value of the power-law slope corresponding to the PSD (α) is listed in Column (8) assuming $\alpha = \beta + 1$. Two fits of the structure function are made for the UVW2 data. (a) corresponds to fitting the SF between 10 and 50 d and (b) corresponds to fitting the data between 50 and 160 d. *A fit to the *V*-band data could not be well constrained. The values shown correspond to the *B*-band SF fit.

(1) Waveband	(2) T (days)	(3) δ (days)	(4) τ_{min} (days)	(5) τ_{max} (days)	(6) β	(7) τ_{char} (days)	(8) α (PSD)
X-ray	3524.232	5.3	10	100	0.14 ± 0.05	−−	1.14
UVW2[a]	3524.232	5.3	10	50	$0.86^{+0.14}_{-0.13}$	34^{+11}_{-5}	1.86
UVW2[b]	3524.232	5.3	50	160	$1.25^{+0.20}_{-0.18}$	112^{+9}_{-7}	2.25
UVM2	3157.063	7.0	10	130	$0.80^{+0.29}_{-0.50}$	63^{+32}_{-21}	1.80
UVW1	3157.063	6.9	10	130	$0.86^{+0.27}_{-0.21}$	66^{+21}_{-14}	1.87
U	3157.063	6.9	10	130	$0.71^{+0.28}_{-0.21}$	71^{+27}_{-18}	1.71
B	3157.063	6.9	10	130	$0.71^{+0.30}_{-0.51}$	59^{+33}_{-19}	1.71
V*	3157.063	6.9	10	130	0.71	59	1.71

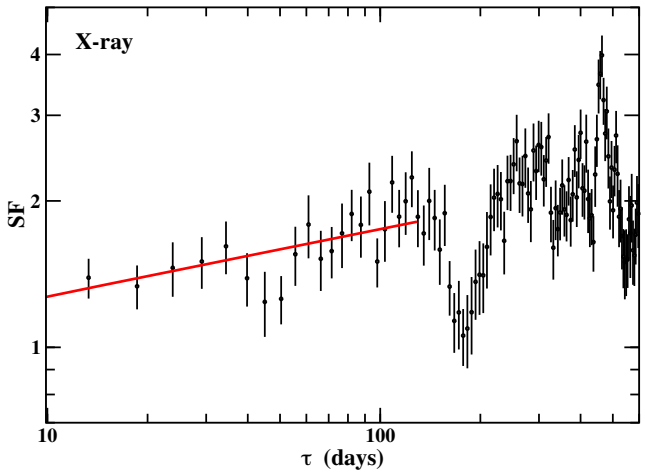

Figure 5. The power law fitted to the X-ray structure function between 10 and 100 d is consistent with a PSD slope of ∼1**.**

UVW2 filter (Wilkins et al. 2015). It could be that the DCF in Year 8 is dominated by this one extreme event making the correlation more significant.

5.3 Correlations between all light curves in Year 2

The monitoring of Mrk 335 during the second year was the most complete as it included measurements in nearly all filters at each epoch. This makes it possible to examine correlations between light curves in the UVW2 and all other UV-optical filters, as well as comparing with the X-rays.

In Fig. 8, the DCF is shown for each UV-optical light curve against the X-rays (left-hand panel) and against the UVW2 (right-hand panel) light curves during Year 2. The DCFs comparing the X-ray variations to the UV-optical light curves show no significant correlations. The strongest peak is seen at ∼95 per cent confidence level in the UVW2 and the UVW1 DCFs (left-hand panel). There is what appears to be a single significant data point in the *V*-band DCF that peaks at negative lag. Given the low-amplitude variability in this band, it seems more likely that the single data point is a spurious event rather than a significant lag. Indeed, if the centroid of the DCF were used to measure the lag rather than the peak (e.g. Welsh 1999), the delay would not be important.

The DCFs comparing the UVW2 light curve with some other UV-optical wavebands (i.e. UVW1, UVM2, U, and B) yield more significant correlations at >95 per cent confidence. The correlation between UVW2 and V are not significant. The correlation between UVW2 and UVM2 is consistent with zero lag. This is expected since both filters examine overlapping parts of the SED.

The peak of the DCFs among UVW2 and UVW1, U, and B, are all offset by ∼5 d, indicating that changes in the shorter wavelength band (UVW2) are the leading variations in other wavebands. As with the 11-yr average DCFs, the lags correspond to one resolution element and are formally consistent with zero. However, seeing the same offset in all the wavebands suggests that that interband lags may be occurring on time-scales shorter than 5 d. Again, more frequent monitoring with shorter cadence may better constrain these lag estimates. There are segments in this *Swift* light curve that are sampled with higher frequency, but these are not sufficient to carry out the analysis.

6 DISCUSSION

The structure function slope (β) and characteristic time-scale (τ_{char}) are determined for the ∼11-yrX-ray and UV-optical light curves of Mrk 335. For the UV-optical light curves, the SF slope is $\beta \approx 0.8$, roughly comparable to a PSD spectral index of $\alpha \approx 1.8$. The values measured for Mrk 335 are within the range of β found for a sample of Seyfert 1 galaxies (CP01) and comparable to the UV-optical PSD ($\alpha \approx 1-2$) often measured for Seyferts (e.g. Krolik et al. 1991; Reichert et al. 1994; McHardy et al. 2004; Arévalo et al. 2008; Breedt et al. 2010). The similarity in the slopes of the UV and the optical SF might suggest a common physical mechanism is at work.

CP01 present only a *V*-band structure function for Mrk 335. A slope of 1.00 ± 0.23 and a characteristic time-scale of 49^{+31}_{-23} days were measured from fitting the SF. Unfortunately, the *Swift V*-band light curve is sparsely sampled and the amplitude of the variations in the band is small, rendering a poorly defined SF. Independent measurements of β and τ_{char} were not possible with the current data. However, the CP01 SF measurements for Mrk 335 are consistent with the values measured here in the other optical bands (B and U).

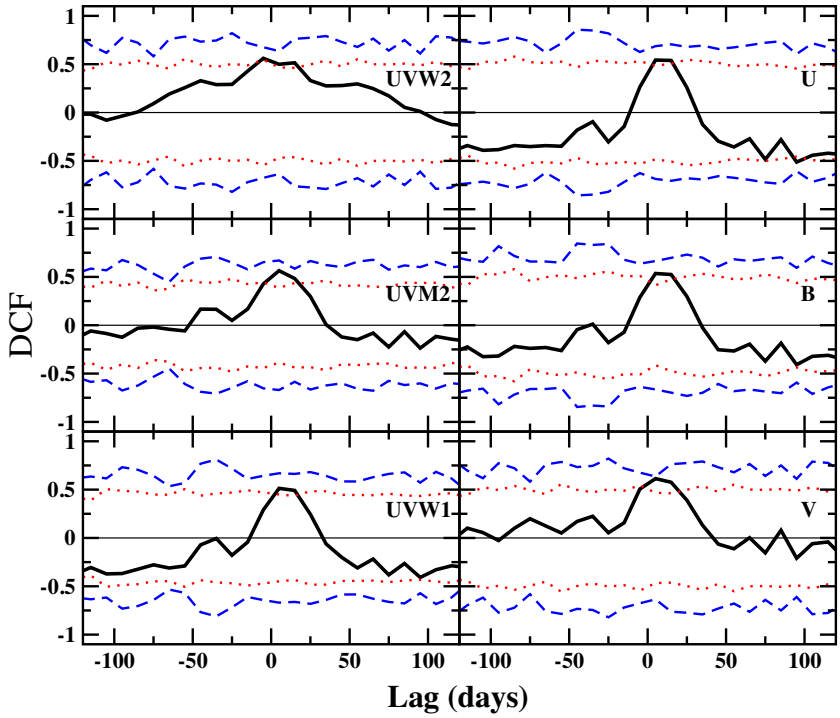

Figure 6. The *Swift* DCFs between the X-rays and the *UVOT* filters over the 11 years of monitoring Mrk 335. Correlations are shown between ±120 d and the positive lags imply that the X-rays are leading the second band (shown in each panel). The horizontal line marks zero correlation, while the dotted-red and the dashed-blue curves denote 95 and 99.9 per cent confidence contours, respectively.

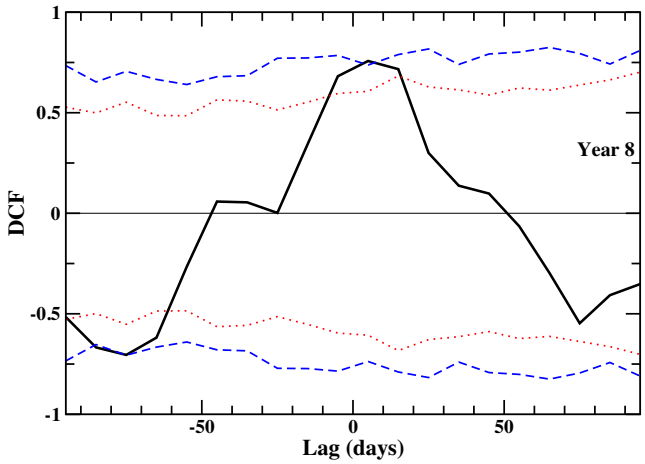

Figure 7. The *Swift* DCF between the X-rays and the UVW2 filter during Year 8 of monitoring Mrk 335. Year 8 exhibits the strongest single-year correlation between the X-ray and the UVW2. Correlations are shown between ±95 d and a positive lag implies that the X-rays are leading the UVW2. The horizontal line marks zero correlation while the dotted-red and the dashed-blue curves denote 95 and 99.9 per cent confidence contours, respectively.

Notably, the AGN Watch[2] monitoring campaign of Mrk 335 was conducted from the late 1980s to the mid 1990s (Kassebaum et al. 1997; Peterson et al. 1998), prior to the NLS1 dropping to its current, long-lasting, low X-ray flux interval. The similarities between the SFs calculated in this work and that of Mrk 335 in the mid 1990s, and those of other Seyfert 1 galaxies, suggest the driving mechanism (i.e. accretion via a standard disc) has not fundamentally changed in Mrk 335 during this extended X-ray low-flux interval. This may support a simple explanation like partial covering of the central region (e.g. Tanaka et al. 2004).

Under the assumption of a standard, Shakura–Sunyaev accretion disc (Shakura & Sunyaev 1973), the temperature profile is

$$T\left(r\right) = \left[\frac{3GM\dot{M}}{8\pi\sigma r^3}\left(1-\sqrt{\frac{r_{isco}}{r}}\right)\right]^{1/4} \quad (2)$$

where σ is the Stefan–Boltzmann constant. At a given distance, the blackbody emission peaks at a wavelength

$$\lambda\left(r\right) \approx \frac{hc}{3kT\left(r\right)} \quad (3)$$

Assuming the efficiency of converting mass to radiation is 0.1, the peak emission observed in a given bandpass will be dominated by thermal emission originating at a distance of

$$\frac{r}{r_g} = \left(1.28\times10^{11}\right)\lambda^{4/3}\left(\frac{M}{10^8\,\mathrm{M}_\odot}\right)^{-1/3}\left(\frac{\dot{M}}{\dot{M}_{Edd}}\right)^{1/3} \times\left(1-\sqrt{\frac{r_{isco}}{r}}\right)^{1/3} \quad (4)$$

where $\dot{M}$ is the accretion rate in units of the Eddington rate $\dot{M}_{Edd}$, λ is in metres, and distance is in gravitational radii ($1r_g = GM/c^2$).

The peak, source-frame, wavelengths in the *Swift UVW2* and the *B* wavebands are 1880 Å and 4280 Å, respectively. For Mrk 335, a black hole mass of $M = 2.6\times10^7\,\mathrm{M}_\odot$ (Grier et al. 2012) and $\dot{M} = 0.2\dot{M}_{Edd}$ is assumed. The emission in the UV and the optical bands is dominated by blackbody emission that is originating at $\sim100r_g$ and $\sim300r_g$, respectively.

[2] http://www.astronomy.ohio-state.edu/~agnwatch/

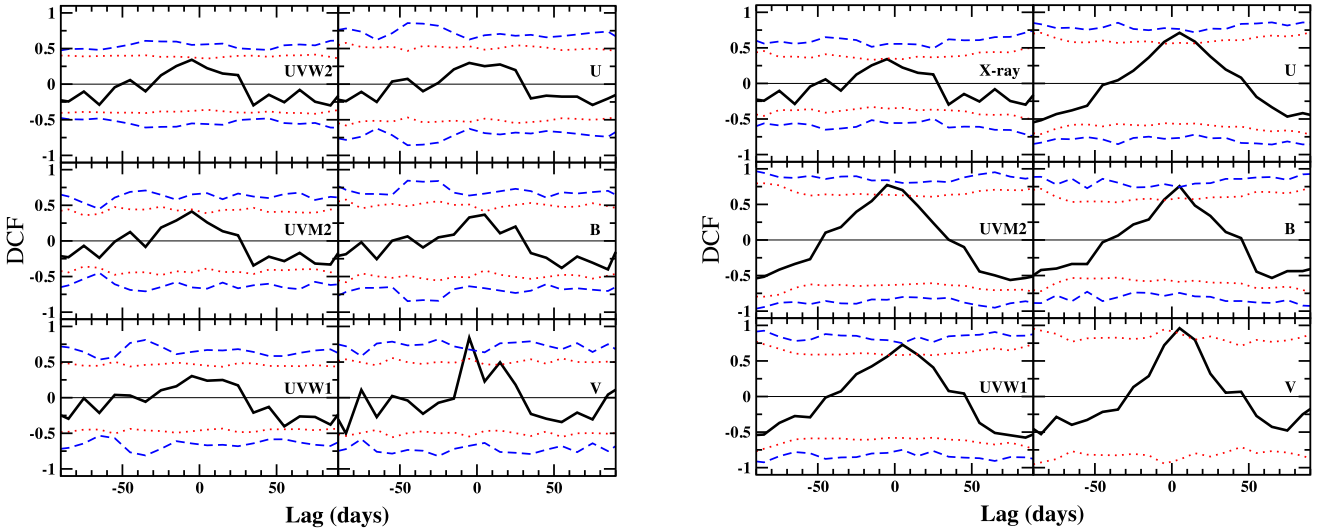

Figure 8. Left-hand panel: The *Swift* DCFs of Mrk 335 for the X-rays and the various *UVOT* filters during Year 2 only. No significant correlations are revealed and the sharp peak in the *V*-band DCF is likely a spurious event. Right-hand panel: The *Swift* DCFs between the UVW2 and all other *UVOT* filters (and X-ray) during Year 2 only. The top-left panel (UVW2 and X-ray) is the same as in the left panel. Correlations among the UVW2 and the UVW1, U, and B wavebands are significant at >95 per cent confidence. In addition, the peaks in these DCFs are offset to a positive lag, which implies the UVW2 variations are leading. Note that the UVM2 shows a peak at zero, which is expected since the wavebands overlap in energy. The correlations with the *V* band are not significant. The horizontal line marks zero correlation while the dotted-red and the dashed-blue curves denote 95 and 99.9 per cent confidence contours, respectively.

The time-scales associated with standard accretion-disc processes can be determined at these distances and compared to the time-scales found in the SF and the DCF analyses. The light crossing time at a distance r around a black hole of mass M is

$$t_{lc} = (5.5 \times 10^{-3}) \left(\frac{M}{10^8\,\mathrm{M}_\odot} \right) \left(\frac{r}{r_g} \right) \mathrm{days} \quad (5)$$

For Mrk 335, $t_{lc} \approx 0.14$ d in the UV region and 0.43 d in the optical region.

The dynamical time-scale is

$$t_{dyn} = (3.7 \times 10^{-2}) \left(\frac{M}{10^8\,\mathrm{M}_\odot} \right) \left(\frac{r}{r_g} \right)^{3/2} \mathrm{days} \quad (6)$$

corresponding to 9.6 d (UV) and 50 d (optical) in Mrk 335.

The thermal time-scale, $t_{th} = t_{dyn}/\alpha_v$, where the viscosity parameter can be taken as $\alpha_v = 0.1$ in a standard accretion disc, will be ∼96 d (UV) and ∼500 d (optical).

Assuming a vertical-to-radial disc ratio of $h/r = 0.01$, the viscous time-scales are $t_{vis} = \frac{t_{th}}{(h/r)^2} \approx 2600$ years and 13600years in the UV and optical regions of Mrk 335, respectively. These time-scales can be off by up to a factor of 10 depending on various assumptions, but generally the viscous time-scales will be much longer than time-scales considered in this work.

In Fig. 9, the characteristic time-scales (τ_{char}) determined from each of the UV-optical structure functions is compared to the accretion-disc time-scales. For all bands, the value of τ_{char} is similar (Table 3), though the UV emission originates a third of the distance closer to the black hole than the optical emission. The optical time-scales agree very well with the orbital time-scales at $300r_g$ in the standard disc. For the UV wavebands, the characteristic time-scales are most likely comparable to the thermal time-scales at $\sim 100r_g$ in a standard accretion disc. Indeed, if uncertainties in the black hole mass were considered, along with the range of radii that are examined in each waveband, then the agreement would be even better.

The *UVW2* light curve of Mrk 335 is of substantial high quality that the SF is rather detailed. The SF appears to possess two breaks in the power spectrum. At short time-scales, the SF seems to match up well with the other bands in terms of its slope, but breaks at a shorter characteristic time-scale of ∼34 d. The function steepens at longer time-scales before again breaking at ∼112 d. Only the longer time-scale is comparable to the thermal time-scales in the UV region of the disc. The shorter break is not comparable to any obvious accretion-disc time-scale and is only consistent with dynamical time-scales at $\sim 230r_g$ or thermal time-scales if α_v were ∼0.3. Both are notably different than the τ_{char} derived from the other UV bands.

The slope of the SF between 10 and 50 d ($\beta = 0.86^{+0.14}_{-0.13}$) is flatter than the slope between 50 and 160 d ($\beta = 1.25^{+0.20}_{-0.18}$). Though both slopes are consistent with the average slope measured in all *UVOT* bands, they are different from each other. This may indicate that the breaks are unique and that the power spectra are arising from independent processes. It could be that the second break exists in all wavebands, but not significantly detected because of limited data or data quality.

CP01 noticed multiple breaks in the optical structure function of NGC 5506 and suggested they may be attributed to starburst activity. Aretxaga et al. (1997) generated models of the expected variability in a young stellar cluster with compact supernova remnants and predicted characteristic time-scales between 85 and 280 d that may be consistent with observations. It is unclear if a similar interpretation can be adopted for the UV variability in Mrk 335 given the low star formation rate implied by its weak polycyclic aromatic hydrocarbon (PAH) emission (e.g. Sani et al. 2010).

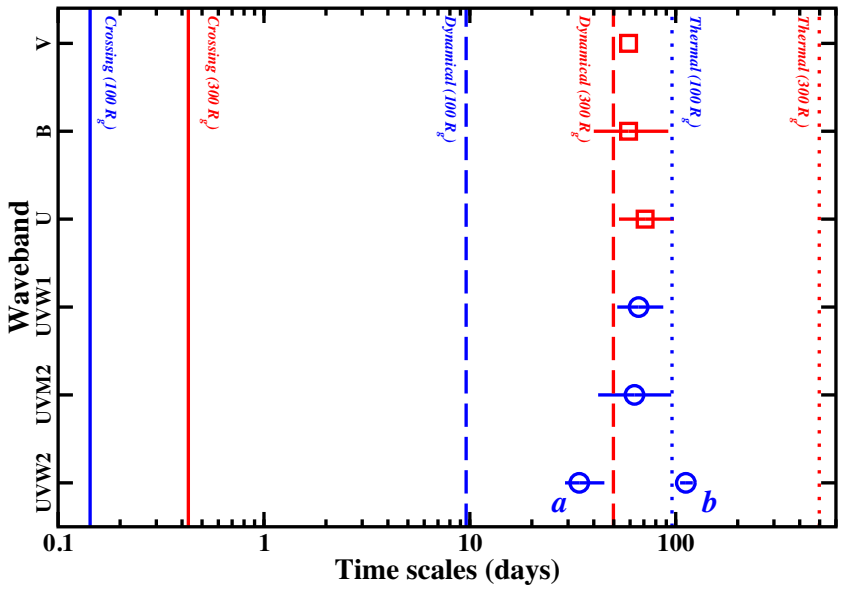

Figure 9. Characteristic time-scales determined from the structure function analysis are compared to the standard accretion-disc time-scales at $100R_g$ (blue lines) and $300R_g$ (red lines). The distances correspond to where the UVW2 and the B wavebands will be dominated by blackbody emission (i.e. UVW2 will be dominated by emission from $\sim 100R_g$ and B from $\sim 300R_g$). The measurements determined from UV light curves are shown with blue circles and those measurements with optical light curves are shown as red squares. Two measurements are shown for the UVW2 with (a) corresponding to fitting the SF between 10 and 50 d ($\tau \approx 34$ d) and (b) corresponding to fitting the data between 50 and 160 d ($\tau \approx 112$ d) to demonstrate the possibility of two distinct slopes and characteristic time-scales in the UVW2 SF. A fit to the *V*-band data point corresponds to the value of τ measured for the *B*-band.

Alternatively, the existence of a compact or abort jet (e.g. Ghisellini, Haardt & Matt 2004) in Mrk 335 as previously suggested (Gallo et al. 2013, 2015; Wilkins et al. 2015) may demand other time-scales are considered. Though Mrk 335 is radio-quiet and not known to have a jet, X-ray flaring during Year 8 (Wilkins et al. 2015; see below) was attributed to collimated, relativistic outflow that could also generate UV emission. Indeed, the DCF between UVW2 and X-rays was strongest in Year 8. The time-scales detected here may be too large even within a jet that cools as it propagates (i.e. with the UV-emitted upstream from the X-ray emission point).

One could examine the UVW2 structure function in individual years to determine any variable behaviour in the function itself. This would be challenging despite how good these data are. Mrk 335 is observed for ∼240 d of each year. The SF is robust within $\sim 0.3T$ (CP01), meaning the slope can be reliably measured up to ∼70 d. Each year would allow investigation of only the short time-scale SF that is apparent in the 11-yrdata set. Moreover, the SF data quality (i.e. resolution and scatter) would be compromised as fewer light curve pairs (i, j) would contribute to each SF bin.

The X-ray structure function has a shallow power-law slope consistent with 0 (flat) between ∼2 and 50 d. There is no observable break, that may be indicative of a turnover occurring at much higher frequencies (Arévalo et al. 2008). Arévalo et al. (2008) measured a break in the power spectrum at $\sim 1.7 \times 10^{-4}$ Hz ($\tau \approx 6000$ s) in the 2006 *XMM–Newton* observation of Mrk 335 when the AGN was in a bright flux state. At lower frequencies the slope was fixed at $\alpha = 1$ though allowing it to vary did not significantly change the value. The time-scale is in relatively good agreement with black hole mass measurements for Mrk 335.

The SF slope measured here is comparable to a PSD slope of ∼1, consistent with the measurements of Arévalo et al. (2008). Assuming the SF power law is comparable to the extrapolation of the flat low-frequency, power-law spectrum measured by Arévalo et al. (2008), there is no strong indication of physical changes in the processes causing the X-ray emission.

The search for correlations and lags in the 11-yrlight curves of Mrk 335 did not yield highly significant results, and most correlations were at the ∼95 per cent confidence level. The lack of strong correlations was consistent with previous findings in Grupe et al. (2012) using a shorter light curve. However, there is evidence that the strength of the correlations between the X-rays and the UVW2 changes across the light curve. For example, in Year 8 of the campaign, the UVW2 and the X-rays were well correlated at ∼99.9 per cent confidence level. There was also a slight shift in the peak of all the DCFs indicating the X-ray variations lead the fluctuations in other lower energies wavebands. In all cases, the shift was equivalent to one resolution element in the DCF (i.e. 5 ± 5 days) and formally consistent with zero lag. However, monitoring with higher cadence could reveal significant correlations.

During Year-8 (2014 August), Mrk 335 exhibited a giant (factor of 10) X-ray flare (Grupe et al. 2014) that triggered a *NuSTAR* target-of-opportunity observation. The X-ray flare was interpreted as vertically collimated outflow moving away from the disc at mildly relativistic speeds (Wilkins et al. 2015). It was noted that the UVW2 emission peaked and diminished along with the X-ray flare, though the flaring in the UV was only at the ∼25 per cent level. Since the number of corona photons striking the disc compared to the total number of corona photons emitted (i.e. the reflection fraction) did not change during the X-ray flare, Wilkins et al. (2015) disfavour X-ray reprocessing as the cause of the UV brightening. Instead, the UV emission could be generated in a jet-like structure through synchrotron self-Compton processes (e.g. Ghisellini et al. 1985).

The data set in Year 2 is important because all the *UVOT* wavebands are equally well sampled in that epoch and correlations between all the wavebands could be investigated. As with the 11-yraverage DCFs, no correlations were found at greater than the 95 per cent confidence level between the X-ray and any of the UV-optical wavebands. However, more significant correlations at >95 per cent confidence level were found between the UVW2 light curve and other UV-optical light curves. Again, a slight offset of one resolution element, corresponding to a lag of 0−5 d is seen with the UVW2 light curve leading the others. The temporal resolution is not sufficient to investigate lags shorter than 5 d, but the time-scales are what may be expected from X-ray reprocessing in the standard accretion disc that follows a $\tau_{\rm lag} \propto \lambda^{4/3}$ relation (e.g. McHardy et al. 2014). Such lags would be short for Mrk 335, only part of a day, but many reverberation studies also show the amplitude of the lags implies discs that are larger than predicted by the standard model (e.g. McHardy et al. 2014; Cackett et al. 2017).

7 CONCLUSIONS

Swift monitoring of Mrk 335 since 2007 while the NLS1 has been in an extended low X-ray-flux state is presented. Analysis of the UV-optical and X-ray structure functions (power spectra) suggests that the AGN is consistent with previous high-flux observations of it, and comparable with other Seyfert 1 galaxies. Variability in the UV and optical emission can be attributed to thermal and dynamic processes in the accretion disc, respectively. The current X-ray low-flux state of Mrk 335 does not appear to be driven by changes in the accretion disc structure or behaviour. The changes originate in the X-ray emitting region and could be attributed to physical changes in the corona or absorption. Interestingly, the UVW2 (∼1800 Å) structure function possesses two breaks and two different slopes indicating multiple physical processes are at work. We speculate that the presence of an unresolved, compact (perhaps aborted) jet may be at work in Mrk 335 and responsible for the appearance of the structure function.

The search for correlations and lags between different energy bands revealed interesting behaviour that should be followed up with more frequent monitoring of Mrk 335 with shorter cadence. Correlations are not significant beyond the ∼95 per cent confidence level when considering the 11-yrlight curves, but more significant behaviour is present when considering segments of the light curves. A correlation between the X-ray and the UVW2 in 2014 (Year-8) may be predominately caused by a giant X-ray flare that was interpreted as a jet-like emission. In 2008 (Year-2), more significant correlations (>95 per cent level) and possible lags between the UVW2 emission and other UV-optical wavebands may be consistent with reprocessing of X-ray/UV emission in the accretion disc.

ACKNOWLEDGEMENTS

We thank the *Swift* team for approving our various ToO requests to monitor Mrk 335 over the years. LCG and DMB are grateful to Dr. Tina Harriott for discussion and support. Many thanks to William Alston and the referee for providing suggestions that improved the manuscript.

REFERENCES

Aretxaga I., Cid Fernandes R., Terlevich R. J., 1997, MNRAS, 286, 271
Arévalo P., McHardy I. M., Summons D. P., 2008, MNRAS, 388, 211
Bauer A., Baltay C., Coppi P., Ellman N., Jerke J., Rabinowitz D., Scalzo R., 2009, ApJ, 696, 1241
Breedt E. et al., 2010, MNRAS, 403, 605
Breeveld A. A. et al., 2010, MNRAS, 406, 1687
Burrows D. et al., 2005, Space Sci. Rev., 120, 165
Cackett E., Chiang C-Y., McHardy I., Edelson R., Goad M., Horne K., Korista K., 2018, ApJ, 857, 53
Cameron D. T., McHardy I., Dwelly T., Breedt E., Uttley P., Lira P., Arevalo P., 2012, MNRAS, 422, 902
Cardelli J. A., Clayton G. C., Mathis J. S., 1989, ApJ, 345, 245
Collier S., Peterson B. M., 2001, ApJ, 555, 775 (CP01)
Di Clemente A., Giallongo E., Natali G., Trevese D., Vagnetti F., 1996, ApJ, 463, 466
Edelson R., Krolik J. H., 1988, ApJ, 333, 646
Edelson R., Turner T. J., Pounds K., Vaughan S., Markowitz A., Marshall H., Dobbie P., Warwick R., 2002, ApJ, 568, 610
Gallo L. C. et al., 2013, MNRAS, 428, 1191
Gallo L. C. et al., 2015, MNRAS, 446, 633
Gallo L. C., 2006, MNRAS, 368, 479
Ghisellini G., Maraschi L., Treves A., 1985, A&A, 146, 204
Ghisellini G., Haardt F., Matt G., 2004, A&A, 413, 535
González-Martín O., 2018, ApJ, 858, 2
Grier C. J. et al., 2012, ApJ, 755, 60
Grupe D., Komossa S., Gallo L. C., 2007, ApJ, 668, L111
Grupe D., Komossa S., Gallo L. C., Fabian A. C., Larsson J., Pradhan A. K., Xu D., Miniutti G., 2008, ApJ, 681, 982
Grupe D., Komossa S., Gallo L. C., Longinotti A. L., Fabian A. C., Pradhan A. K., Gruberbauer M., Xu D., 2012, ApJS, 199, 28
Grupe D., Gallo L., Komossa S., 2014, ATel, 6468, 1
Hill J. E. et al., 2004, SPIE, 5165, 217
Hufnagel B. R., Bregman J., 1992, ApJ, 386, 473
Hughes P. A., Aller H. D., Aller M. F., 1992, ApJ, 396, 469
Kara E., Fabian A. C., Cackett E. M., Uttley P., Wilkins D. R., Zoghbi A., 2013, MNRAS, 434, 1129
Kassebaum T. M., Peterson B. M., Wanders I., Pogge R. W., Bertram R., Wagner R. M., 1997, ApJ, 475, 106
Kawaguchi T., Mineshige S., Umemura M., Turner E. L., 1998, ApJ, 504, 671
Komossa S. et al., 2017, IAUS, 324, 168
Komossa S., Grupe D., Saxton R., Gallo L., 2014, Proceedings of Swift: 10 Years of Discovery (SWIFT 10), id. 143
Krolik J. H., Horne K., Kallman T. R., Malkan M. A., Edelson R. A., Kriss G. A., 1991, ApJ, 371, 541
Longinotti A. L. et al., 2013, ApJ, 766, 104
Longinotti A. L., Nucita A., Santo-Lleo M., Guainazzi M., 2008, A&A, 484, 311
McHardy I. M. et al., 2014, MNRAS, 444, 1469
McHardy I. M., Papadakis I. E., Uttley P., Page M. J., Mason K. O., 2004, MNRAS, 348, 783
McHardy I. M., Koerding E., Knigge C., Uttley P., Fender R. P., 2006, Nature, 444, 730
Middei R. Vagnetti F., Bianchi S., La Franca F., Paolillo M., Ursini F., 2017, A&A, 599, 82
Mushotzky R. F., Edelson R., Baumgartner W., Gandhi P., 2011, ApJ, 743, 12
Paltani S., 1999, in Takalo L., Sillanpää A., eds, ASP Conf. Ser, 159, San Francisco, p. 293
Peterson B. M., Wanders I., Bertram R., Hunley J. F., Pogge R. W., Wagner R. M., 1998, ApJ, 501, 82
Poole T. S. et al., 2008, MNRAS, 383, 627
Reichert G. A. et al., 1994, ApJ, 425, 582
Robertson D. R. S, Gallo L. C., Zoghbi A., Fabian A. C., 2015, MNRAS, 453, 3455
Roming P. W. A. et al., 2009, ApJ, 690, 163
Roming P. W. A. et al., 2005, Space Sci. Rev., 120, 95
Sani E., Lutz D., Risaliti G., Netzer H., Gallo L.C., Trakhtenbrot B., Sturm E., Boller T., 2010, MNRAS, 403, 1246
Schlegel D. J., Finkbeiner D. P., Davis M., 1998, ApJ, 500, 525

Shakura N. I., Sunyaev R. A., 1973, A&A, 24, 337
Shappee B. J. et al., 2014, ApJ, 788, 48
Simonetti J. H., Cordes J. M., Heeschen D. S., 1985, ApJ, 296, 46
Tanaka Y., Boller Th., Gallo L., Keil R., Ueda Y., 2004, PASJ, 56, 9
Timmer J., König M., 1995, A&A, 300, 707
Vagnetti F., Middei R., Antonucci M., Paolillo M., Serafinelli R., 2016, A&A, 593, 55
Vanden Berk D. E. et al., 2004, ApJ, 601, 692
Vaughan S., Edelson R., Warwick R. S., Uttley P., 2003, MNRAS, 345, 1271
Welsh W. F., 1999, PASP, 111, 1347
Wilkins D. R., Gallo L. C., 2015, MNRAS, 449, 129
Wilkins D. R., Gallo L. C., Grupe D., Bonson K., Komossa S., Fabian A. C., 2015, MNRAS, 454, 4440

SUPPORTING INFORMATION

Supplementary data are available at *MNRAS* online.

Table1.tex
Table2.tex

Please note: Oxford University Press is not responsible for the content or functionality of any supporting materials supplied by the authors. Any queries (other than missing material) should be directed to the corresponding author for the article.

This paper has been typeset from a TEX/LATEX file prepared by the author.